ECS Transactions, 80 (5) 67-75 (2017)
10.1149/08005.0067ecst ©The Electrochemical Society

Nanostructures for Reduced Lattice Thermal Conductivity — Case Studies for Nanopores and Grain Boundaries

Qing Hao, Dongchao Xu, Yue Xiao, Bo Xiao, and Hongbo Zhao

Department of Aerospace and Mechanical Engineering, University of Arizona, Tucson, AZ 85721, USA

Solid-state thermoelectric devices have the ability to directly convert heat into electricity for power generation. A good TE material should possess a high electrical conductivity, a high Seebeck coefficient, and a low thermal conductivity. This requirement is hard to be satisfied within the same material. To address this issue, the nanostructuring approach has been widely used to reduce the lattice part of the thermal conductivity (k_L) but still maintain the bulk electrical properties. High TE performance has thus been achieved in various nanostructured materials, such as nanoporous thin films and different nanostructured bulk materials. To better understand the observed k_L reduction by nanostructures, two major types of nanostructured materials are studies here, including nanoporous thin films and nanograined bulk materials. In the latter case, a super-flexible thin film was hot pressed onto a wafer to represent a grain boundary.

Introduction

Solid-state thermoelectric (TE) devices have the ability to directly convert heat into electricity for power generation [1]. In recent years, TE devices have had renewed interest as sustainable energy sources due to attractive features such as high reliability, environmental friendliness, and the absence of moving parts. In physics, the performance of TE materials is evaluated by their TE figure of merit (ZT), defined as ZT = $S^2\sigma T/k$, where S, σ, k, and T represent Seebeck coefficient, electrical conductivity, thermal conductivity, and absolute temperature, respectively. Here k can be further split into the lattice contribution k_L and the electronic contribution k_E. The challenge of TE research lies in achieving a high power factor $S^2\sigma$ but a low k within the same material. This largely limits the choices for high-performance and earth-abundant TE materials. Currently, dominant TE materials are still heavily based on toxic, rare and expensive elements such as tellurium.

Instead of looking for new compounds and their alloys, ZTs of existing materials can be largely enhanced using the nanostructuring approach [2]. In such materials, the structure sizes should be shorter than majority phonon mean free paths (MFPs) to suppress k_L but still longer than majority electron MFPs to maintain bulk-like electrical properties, leading to enhanced ZTs. A high ZT can be achieved in conventional TE materials such as bulk BiSbTe alloys [3] and PbTe [4]. Despite many exciting results, a fundamental understanding of the observed k_L reduction by various nanostructures is still lacking. In this work, two important nanostructures are studied for their impact on phonon transport, namely periodic nanopores within a thin film and nanograins within a

Downloaded on 2017-11-30 to IP 150.135.165.21 address. Redistribution subject to ECS terms of use (see ecsdl.org/site/terms_use) unless CC License in place (see abstract).

bulk material. Due to the challenge in measuring a single grain boundary (GB) in a bulk material, a thin film was hot pressed onto a wafer to represent a GB. These two topics are separately described in the following two sections.

Case 1: Thermal Investigation of Nanoporous Thin Films

Review of Existing Work on Nanoporous Si Thin Films

In the last decade, micro- and nano-porous Si thin films were intensively studied for TE applications because of the low price and abundance of Si ([5-20]). In nanofabrication, the porous patterns were first defined by lithography [5, 8, 11, 14, 15, 17, 18], a superlattice nanowire pattern transfer technique [9], self-assembled block copolymer [10, 19], or a monolayer film of polystyrene spheres [10]. Pores were then drilled with dry etching, i.e., reactive ion etching (RIE) or deep reactive ion etching (DRIE). In more recent work, >100 nm pores were also drilled with a focused ion beam (FIB) [16]. With nanopores, ZTs were enhanced with bulk-like electrical properties and significantly reduced k_L. For a film with hexagonally packed pores, room-temperature ZT~0.4 was reported based on electrical and thermal properties separately measured with similar samples [10], compared with ZT~0.01 for solid Si films.

Theoretically, it is found that the measured k_L values can be much lower than that predicted by phonon transport analysis that assumed completely diffusive phonon scattering on pore edges along with the bulk phonon dispersion and MFPs [11]. In some studies, such divergence was attributed to the coherent phonon transport within the periodic nanoporous structure. In this situation, the phonon dispersion should be modified, resulting in reduced phonon group velocities and thus k_L. This so-called “phononic effect” was widely studied for superlattices with atomically smooth interfaces, in which phonon coherence became dominant for <5 nm periods at 300 K [21, 22]. In contrast to superlattices, the measured nanoporous films still have large feature sizes, with amorphous pore edges to destroy the phonon phase and thus phononic effects. The frequency of phonons impacted by the periodic structure can be approximated as $f = \pi v_{avg}/P$, in which v_{avg} is the averaged sound velocity and P is the period [23]. For nanoporous Si films with a period of ~100 nm, only phonons below ~200 GHz can be impacted, instead of majority heat-carrying phonons at a few THz. The overall impact on k_L is negligible. Earlier calculations for nanoporous films with >100 nm feature sizes indicated negligible phononic effects [24]. Along this line, the analysis of nanoporous thin films with a ~34 nm period [9] still suggested incoherent phonon transport, with slightly increased effective pore sizes due to pore-edge amorphization [25].

The divergence between theoretical analysis and experiments is partially due to the challenges in accurately measuring k of thin films. In many studies, a thin film was loaded onto a microdevice, in which two suspended membranes were bridged by the measured thin film. Metal coils were fabricated on both membranes as both the heater and thermometer. Such a device may have a large thermal contact resistance between the device and the measured thin film, leading to underestimated k in measurements. In addition, the possible damage of the fragile nanoporous thin film during the sample transfer may also reduce the measured k values. The above-mentioned k underestimation was observed by k measured for nanoporous Si thin films by the same authors [10, 19]. By loading a thin film onto a microdevice, room-temperature k values were 1.14–2.03 W/m·K for samples with 55-nm pitch and 23-nm neck between adjacent pores [10]. By fabricating the measured thin film into a suspended device, the impact of sample-device thermal contact was eliminated and this new setup gave a higher k~1.8 W/m·K for 60-

Downloaded on 2017-11-30 to IP 150.135.165.21 address. Redistribution subject to ECS terms of use (see ecsdl.org/site/terms_use) unless CC License in place (see abstract).

nm-pitched nanoporous patterns with an even smaller neck width (16 nm) and strong defect scattering of phonons using ion implantation for doping [19].

To provide better guidance for the future thermal studies of nanoporous thin films, here the in-plane k for nanoporous Si thin films and cross-plane k for $In_{0.1}Ga_{0.9}N$ thin films were measured. It is found that the measurement results can be well explained with diffusive phonon scattering by pore edges, without considering phononic effects.

In-Plane k Measurements of a Nanoporous Si Thin Film

Figure 1 shows the employed measurement setup for nanoporous Si thin films. The 220-nm-thick nanoporous Si film was fabricated from the device layer of a silicon-on-insulator (SOI) wafer, with DRIE-drilled pores. As the heater/thermometer, a 10-nm-thick Cr adhesion layer followed by 40-nm-thick Pt were coated onto the device. The film was suspended by etching off the underlying oxide layer. Such an integrated setup eliminated the influence of sample-device thermal contact. The same measurements were reported in our earlier studies but RIE was used to pattern the pores, with some overetching on the top of a pore [5].

The in-plane k of the nanoporous film was measured based on ac self-heating (i.e., 3ω technique) of a suspended structure [26], which was often more accurate than previous nanoporous film studies using dc heating [15]. In 3ω measurements, an ac current was passed mainly through the metal layer on the Si film. The temperature along the film oscillated and was sensed by the 3ω voltage ($V_{3\omega}$) across the film. By fitting the frequency-dependent $V_{3\omega}$ and its phase, the effective in-plane thermal conductance G and specific heat C_p were determined for the bilayer film. The metal-layer contribution to G was estimated using the measured electrical conductance G_e of this layer, where the Wiedemann–Franz law [27] suggested $k=L\sigma T$ and thus $G_{th}=LG_eT$. The constant L was determined as 4.7×10^{-8} $W\Omega/K^2$, as measured for a suspended Cr/Pt layer. The L value was close to measurements carried out for similar polycrystalline metal films [28]. With a fixed porosity Φ~20%, 2–4 samples were measured for each of the four nanoporous patterns, with pore diameters as 50, 100, 200, and 300 nm. For the extracted in-plane k of the Si film, the standard deviation was 2–4.6% of the k value averaged over different samples, indicated by error bars in Fig. 2.

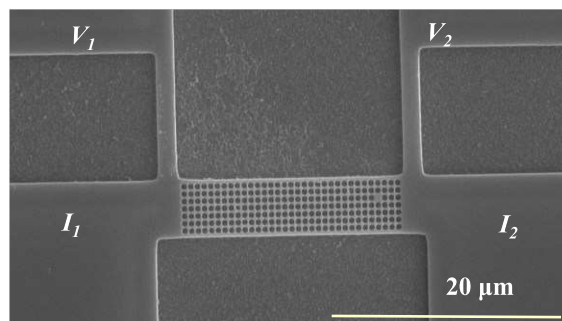

Figure 1. A suspended nanoporous Si film with four electrical probes for thermal measurements.

Figure 2 compares our new measurements and previous measurements (symbols) with k_L predicted by two-dimensional phonon Monte Carlo simulations that assume bulk-like phonon transport and diffusive phonon scattering by pore edges. Only the porosity Φ=20% is computed as the line in Fig. 2 [6, 7, 29], whereas previous measurements cover Φ of 7–64%. In general, the simulations agree well with the new measurement,

Downloaded on 2017-11-30 to IP 150.135.165.21 address. Redistribution subject to ECS terms of use (see ecsdl.org/site/terms_use) unless CC License in place (see abstract).

following the same trend as existing studies with Φ of 7–38% [8, 14, 17, 19]. These consistent measurements are all based on a device directly fabricated from the measured nanoporous thin film. Such measurements avoid the sample-device thermal contact problem and possible sample damage during film transfer.

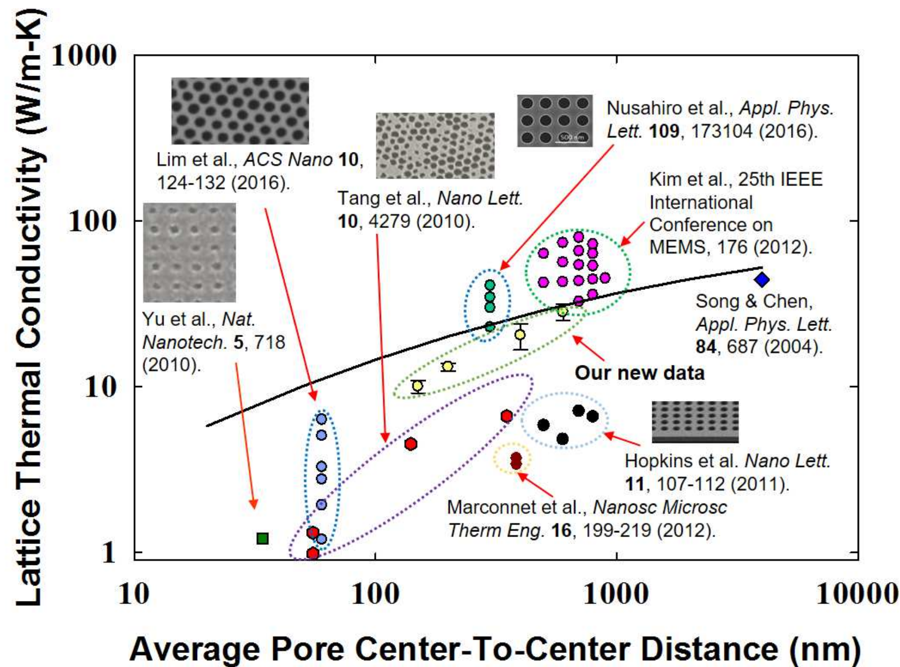

Figure 2. Comparison between predicted (Φ=20%) and measured in-plane k_L of porous Si films at 300 K, except for Hopkins *et al*. measuring the cross-plane k.

Cross-Plane k Measurements of a $In_{0.1}Ga_{0.9}N$ Thin Film

Unrestricted to nanoporous Si films, similar studies were also performed on nanoporous $In_{0.1}Ga_{0.9}N$ thin films that can be used for on-chip TE cooling to effectively remove heat from the hot spot within GaN-based transistors. To integrate such TE coolers with a GaN transistor, the selected TE materials should have a thermal expansion coefficient similar to that for GaN for better compatibility. Correspondingly, GaN-based alloys are recommended for such TE devices [30]. For GaN alloys, the power factor $S^2\sigma$ can be better than those for the state-of-the-art high-temperature TE materials such as Si_xGe_{1-x} alloys [31]. Following this, an even high ZT can be achieved in nanoporous films of GaN alloys.

Figures 3a and 3b show the scanning electron microscopy (SEM) images of representative nanoporous films. Different from reported nanoporous Si films with nanofabricated pores [5, 8-11, 14, 15, 17-19], our $In_{0.1}Ga_{0.9}N$ films were directly grown on the substrate, with the nanopores defined by SiO_2 pillars as masks. For all patterns, the pore diameters were fixed at 300 nm and the pores were located on either a square lattice or hexagonal lattice. All layers were grown with unintentional doping. Prior to the growth, the sapphire substrate was heated in H_2 ambient at 1000°C for 3 min to remove surface contaminations. The growth of the structure began with a 50-nm-thick low temperature GaN nucleation layer grown at about 500°C for 3.5 min. Following this, a 50 nm GaN buffer layer was grown at 1060°C for 1 min. Afterwards, the growth was completed by deposition of 150 nm $In_{0.1}Ga_{0.9}N$ layer at 805°C for 60 min. After the high-temperature

Downloaded on 2017-11-30 to IP 150.135.165.21 address. Redistribution subject to ECS terms of use (see ecsdl.org/site/terms_use) unless CC License in place (see abstract).

growth, SiO_2 nanopillars were removed with hydrogen fluoride (HF) to obtain the nanoporous pattern. In contrast with nanofabricated pores, directly grown nanopores have minimized pore-edge defects to eliminate the influence of amorphous pore edges on *k*, as proposed for nanoporous Si films [25].

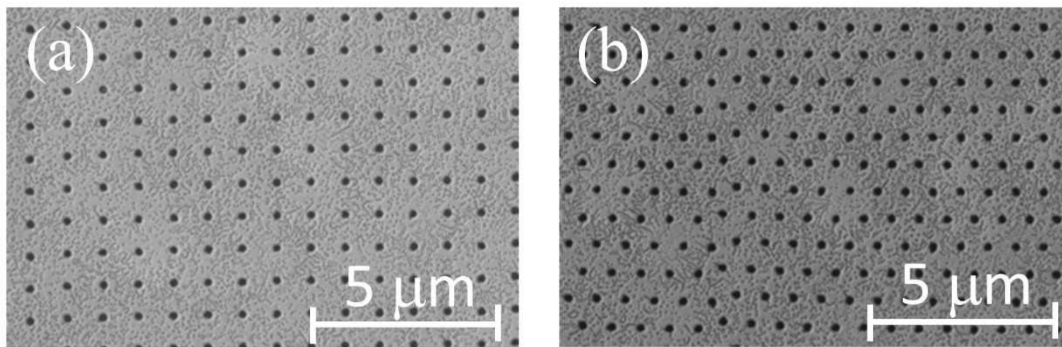

Figure 3. SEM images of nanoporous $In_{0.1}Ga_{0.9}N$ films with (a) aligned pores or (b) hexagonally aligned pores.

Cross-plane *k* has been measured for fabricated $In_{0.1}Ga_{0.9}N$ thin films via the time-domain thermoreflectance (TDTR) method. TDTR is an optical-based, accurate, and robust technique applicable of probing various thermal properties, including thermal conductivity, interfacial thermal conductance, and heat capacity of sample systems ranging from thin films, bulk substrates, to nanoparticles. Prior to thermal measurements, a 55-nm-thick layer of aluminum was coated onto the whole wafer by electron beam deposition to serve as the optical transducer.

Figure 4 shows the measured cross-plane *k* (symbols) compared to phonon transport modeling (line) assuming bulk phonon MFPs and diffusive pore-edge phonon scattering. The uncertainty due to thermal penetration into the substrate is indicated with error bars. In general, the experimental data agree well with the modeling. More details for the modeling and experiments can be found elsewhere [32].

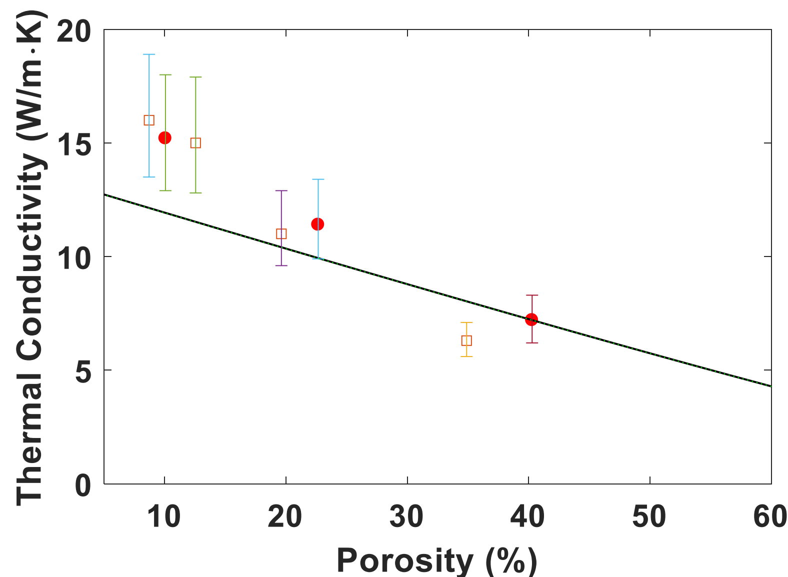

Figure 4. Comparison between the measured and predicted *k* values for tri-layered nanoporous GaN-based films. Here filled circles are for hexagonal patterns, whereas empty squares are for patterns on a square lattice.

Downloaded on 2017-11-30 to IP 150.135.165.21 address. Redistribution subject to ECS terms of use (see ecsdl.org/site/terms_use) unless CC License in place (see abstract).

Case 2: Film-Wafer Bonding to Study Phonon Transport across a Single GB

Bulk and thin-film materials with nano- to micro-grains are widely studied in various research fields. With a high volumetric density of GBs, phonon transport within these materials are strongly suppressed by the GB transmission or reflection of incident phonons, leading to an interfacial thermal resistance R_K known as the Kapitza resistance [27]. The reduction of lattice thermal conductivity k_L by GBs has been exploited to improve thermal insulation and TE materials. Conversely, R_K for GBs and other interfaces can significantly impede heat spreading in electronic devices and thus create challenges for thermal management [33, 34].

One basic GB configuration is a twist GB, in which two identical crystals are rotated relatively around an axis that is perpendicular to the GB plane. Due to the challenge in measuring a single GB within a three-dimensional bulk material, bonding between identical wafers with relative rotation has been employed to represent twisted GBs [35, 36]. Good bonding across the whole wafer, however, is hard to obtain because it requires both wafers to be atomically flat. In contrast, the use of super-flexible thin films ensures a large initial contact area and negligible separation or fracture during the hot press. As one example, extremely high-quality bonding (~1 nm thick interface region shown by high-resolution transmission electron microscopy) has been demonstrated between a 200-nm-thick and millimeter-sized Si membrane and a Ge wafer [37]. With a modest pressure (1.5–2 MPa), superlattices of stacked nano-membranes have been pressed at 200°C to achieve a cross-plane k_L below 2 W/m·K [38].

Figure 5a shows the SEM image of two parallel Si films bonded onto a Si substrate by hot press. The inset is the cross-sectional SEM image to show the high-quality interface. At 300 K, the obtained film-on-substrate structure was measured with an offset 3ω method [39]. For electrical insulation, the wafer was uniformly coated with a thin SiO_2 layer before depositing a 40-μm-wide Cr/Au line used for 3ω measurements (Location A in Fig. 5b inset). As a reference sample, an identical metal line was also patterned in the region without the Si film (Location B). Between the two comparison measurements, the in-phase ac temperature oscillation ΔT_{AC} is shifted by $P(R_{Film}+R_K)/A$ at all frequencies (Fig. 5b). Here P and A are the heating power and area of the metal line, respectively. The cross-plane thermal resistance of the film, R_{Film}, is estimated with the computed cross-plane k for the given film thickness [40].

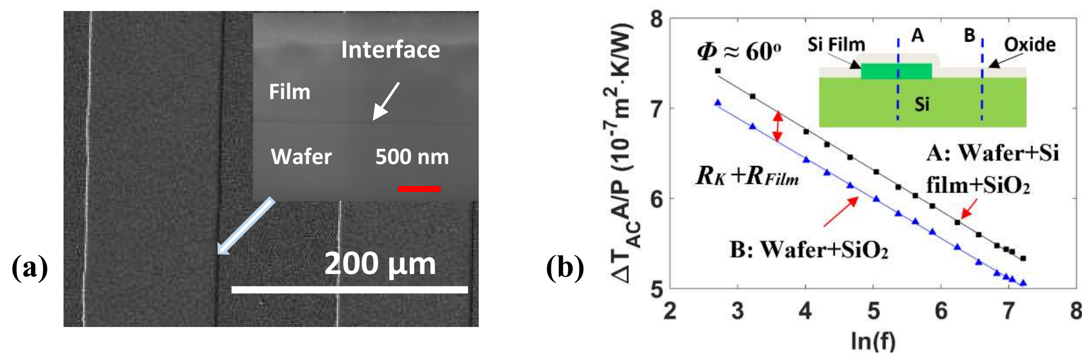

Figure 5. (a) Parallel single-crystal Si thin films bonded onto a Si wafer. (b) ΔT_{AC} of comparison 3ω tests.

Downloaded on 2017-11-30 to IP 150.135.165.21 address. Redistribution subject to ECS terms of use (see ecsdl.org/site/terms_use) unless CC License in place (see abstract).

Thermal investigation of twist GBs was performed with a 70-nm-thick (100) Si thin film hot pressed onto a (100) Si wafer. The film transfer was carried out in diluted HF acid to avoid surface oxidation. After the transfer, the film was annealed at 200°C before hot press to ensure good contact between the sample and the substrate. Under N_2 protection, the film-wafer bonding formed by hot pressing the sample at ~950°C for 1 minute, with rapid heating by an induction heater. Roughly 50 MPa pressure was uniformly distributed across the film by a graphite foil. After measuring R_K, the samples were sealed in a vacuum tube and annealed at 900°C for 1 hour. The interfacial R_K was re-measured after annealing.

For the 70 nm film thickness, ballistic phonon transport is dominant at 300 K. In estimation, R_{Film} is 2.8 m^2·K/GW assuming ballistic phonon transport and the real phonon dispersion in the k space [41]. This value is very close to 2.7 m^2·K/GW estimated with computed cross-plane k [40], indicating little uncertainty in the R_K extraction.

In Fig. 6, the experimental results are plotted as a function of the twist angle between the film and the wafer. After annealing, the R_K values are comparable to measurements on Al_2O_3 wafers bonded at 1400°C for 2 hours [35]. However, the values are still higher than predictions by molecular dynamics simulations that do not consider structural defects in real twist Si GBs [42].

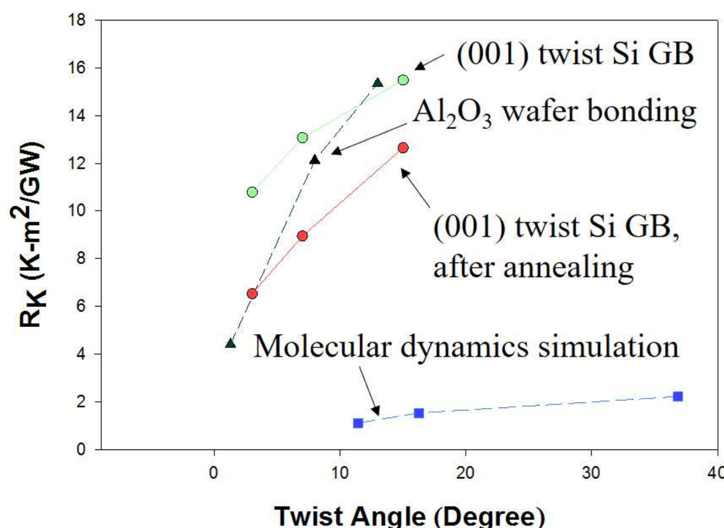

Figure 6. Comparison between measured and predicted R_K values of twist GBs.

Summary

In this work, two important nanofeatures are studied for their impact on k_L, namely nanopores and GBs. It is found that pore-edge diffusive phonon scattering can be sufficient to explain the experimental results of nanoporous Si and $In_{0.1}Ga_{0.9}N$ films, without introducing phononic effects. On the other hand, phonon transport across a twist GB can be more complicated due to interfacial defects and disorder for real samples. The planar film-wafer interface may also be different from real three-dimensional GBs with a high curvature [33]. More studies should be carried out in the future on how the detailed atomic and nanoscale structures on a GB can affect the phonon transport.

Downloaded on 2017-11-30 to IP 150.135.165.21 address. Redistribution subject to ECS terms of use (see ecsdl.org/site/terms_use) unless CC License in place (see abstract).

Acknowledgments

This work is supported by National Science Foundation CAREER Award (grant number CBET-1651840) and AFOSR YIP Award (award number FA9550-16-1-0025).

References

1. H. J. Goldsmid, *Thermoelectric Refrigeration*, Plenum, New York (1964).
2. A. J. Minnich, M. S. Dresselhaus, Z. F. Ren and G. Chen, *Energy & Environmental Science*, **2**, 466 (2009).
3. B. Poudel, Q. Hao, Y. Ma, Y. Lan, A. Minnich, B. Yu, X. Yan, D. Wang, A. Muto, D. Vashaee, X. Chen, J. Liu, M. S. Dresselhaus, G. Chen and Z. Ren, *Science*, **320**, 634 (2008).
4. K. Biswas, J. He, I. D. Blum, C.-I. Wu, T. P. Hogan, D. N. Seidman, V. P. Dravid and M. G. Kanatzidis, *Nature*, **489**, 414 (2012).
5. Q. Hao, D. Xu and H. Zhao, in *2015 MRS Spring Meeting & Exhibit*, P. Hopkins Editor, p. mrss15, San Francisco, California (2015).
6. Q. Hao, G. Chen and M.-S. Jeng, *J. Appl. Phys.*, **106**, 114321 (2009).
7. Q. Hao, Y. Xiao and H. Zhao, *J. Appl. Phys.*, **120**, 065101 (2016).
8. D. Song and G. Chen, *Appl. Phys. Lett.*, **84**, 687 (2004).
9. J.-K. Yu, S. Mitrovic, D. Tham, J. Varghese and J. R. Heath, *Nature Nanotechnology*, **5**, 718 (2010).
10. J. Tang, H.-T. Wang, D. H. Lee, M. Fardy, Z. Huo, T. P. Russell and P. Yang, *Nano Letters*, **10**, 4279 (2010).
11. P. E. Hopkins, C. M. Reinke, M. F. Su, R. H. Olsson, E. A. Shaner, Z. C. Leseman, J. R. Serrano, L. M. Phinney and I. El-Kady, *Nano Letters*, **11**, 107 (2010).
12. J. H. Lee, J. Grossman, J. Reed and G. Galli, *Appl. Phys. Lett.*, **91**, 223110 (2007).
13. J. H. Lee, G. A. Galli and J. C. Grossman, *Nano Letters*, **8**, 3750 (2008).
14. B. Kim, J. Nguyen, P. J. Clews, C. M. Reinke, D. Goettler, Z. C. Leseman, I. El-Kady and R. Olsson, in *Micro Electro Mechanical Systems (MEMS), 2012 IEEE 25th International Conference on*, p. 176 (2012).
15. A. M. Marconnet, T. Kodama, M. Asheghi and K. E. Goodson, *Nanoscale and Microscale Thermophysical Engineering*, **16**, 199 (2012).
16. S. Alaie, D. F. Goettler, M. Su, Z. C. Leseman, C. M. Reinke and I. El-Kady, *Nature Communications*, **6**, 7228 (2015).
17. M. Nomura, J. Nakagawa, K. Sawano, J. Maire and S. Volz, *Appl. Phys. Lett.*, **109**, 173104 (2016).
18. M. R. Wagner, B. Graczykowski, J. S. Reparaz, A. El Sachat, M. Sledzinska, F. Alzina and C. M. Sotomayor Torres, *Nano Letters*, **16**, 5661 (2016).
19. J. Lim, H.-T. Wang, J. Tang, S. C. Andrews, H. So, J. Lee, D. H. Lee, T. P. Russell and P. Yang, *ACS Nano*, **10**, 124 (2016).
20. M. Maldovan, *Phys. Rev. Lett.*, **110**, 025902 (2013).
21. J. Garg and G. Chen, *Phys. Rev. B*, **87**, 140302 (2013).
22. J. Ravichandran, A. K. Yadav, R. Cheaito, P. B. Rossen, A. Soukiassian, S. J. Suresha, J. C. Duda, B. M. Foley, C.-H. Lee, Y. Zhu, A. W. Lichtenberger, J. E. Moore, D. A. Muller, D. G. Schlom, P. E. Hopkins, A. Majumdar, R. Ramesh and M. A. Zurbuchen, *Nat Mater*, **13**, 168 (2014).
23. P. E. Hopkins, L. M. Phinney, P. T. Rakich, R. Olsson III and I. El-Kady, *Applied Physics A*, **103**, 575 (2011).

Downloaded on 2017-11-30 to IP 150.135.165.21 address. Redistribution subject to ECS terms of use (see ecsdl.org/site/terms_use) unless CC License in place (see abstract).

24. A. Jain, Y.-J. Yu and A. J. McGaughey, *Phys. Rev. B*, **87**, 195301 (2013).
25. N. K. Ravichandran and A. J. Minnich, *Phys. Rev. B*, **89**, 205432 (2014).
26. L. Lu, W. Yi and D. Zhang, *Review of Scientific Instruments*, **72**, 2996 (2001).
27. G. Chen, *Nanoscale Energy Transport and Conversion: A Parallel Treatment of Electrons, Molecules, Phonons, and Photons*, Oxford University Press, New York (2005).
28. H. Wang, J. Liu, X. Zhang and K. Takahashi, *International Journal of Heat and Mass Transfer*, **66**, 585 (2013).
29. Q. Hao and G. Chen, in *Applications of Monte Carlo Method in Science and Engineering*, S. Mordechai Editor, InTech (2011).
30. W. Liu and A. A. Balandin, *Journal of Applied Physics*, **97**, 123705 (2005).
31. E. N. Hurwitz, M. Asghar, A. Melton, B. Kucukgok, L. Su, M. Orocz, M. Jamil, N. Lu and I. T. Ferguson, *Journal of Electronic Materials*, **40**, 513 (2010).
32. D. Xu, Q. Wang, X. Wu, J. Zhu, H. Zhao, B. Xiao, X. Wang, X. Wang and Q. Hao, *Frontiers in Energy*, in press (2017).
33. D. G. Cahill, P. V. Braun, G. Chen, D. R. Clarke, S. Fan, K. E. Goodson, P. Keblinski, W. P. King, G. D. Mahan, A. Majumdar, H. J. Maris, S. R. Phillpot, E. Pop and L. Shi, *Applied Physics Reviews*, **1**, 011305 (2014).
34.D. G. Cahill, W. K. Ford, K. E. Goodson, G. D. Mahan, A. Majumdar, H. J. Maris, R. Merlin and S. R. Phillpot, *J. Appl. Phys.*, **93**, 793 (2003).
35. K. Tai, A. Lawrence, M. P. Harmer and S. J. Dillon, *Appl. Phys. Lett.*, **102**, 034101 (2013).
36. D. H. Hurley, M. Khafizov and S. Shinde, *Journal of Applied Physics*, **109**, 083504 (2011).
37. A. M. Kiefer, D. M. Paskiewicz, A. M. Clausen, W. R. Buchwald, R. A. Soref and M. G. Lagally, *ACS nano*, **5**, 1179 (2011).
38. D. Grimm, R. B. Wilson, B. Teshome, S. Gorantla, M. H. Rümmeli, T. Bublat, E. Zallo, G. Li, D. G. Cahill and O. G. Schmidt, *Nano Letters*, **14**, 2387 (2014).
39. D. G. Cahill, M. Katiyar and J. R. Abelson, *Physical Review B*, **50**, 6077 (1994).
40. C. Jeong, S. Datta and M. Lundstrom, *J. Appl. Phys.*, **111**, 093708 (2012).
41. Q. Hao, D. Xu, N. Lu and H. Zhao, *Phys. Rev. B*, **93**, 205206 (2016).
42. S.-H. Ju and X.-G. Liang, *Journal of Applied Physics*, **113**, 053513 (2013).

Downloaded on 2017-11-30 to IP 150.135.165.21 address. Redistribution subject to ECS terms of use (see ecsdl.org/site/terms_use) unless CC License in place (see abstract).